Ji *et al.*
Chinese Journal of Mechanical Engineering (2023) 36:1
https://doi.org/10.1186/s10033-022-00826-w

Chinese Journal of Mechanical Engineering

REVIEW

Open Access

Multiscale Theories and Applications: From Microstructure Design to Macroscopic Assessment for Carbon Nanotubes Networks

Jiachao Ji[1], Yulin Jin[1], Anping Hua[1], Chunhua Zhu[1] and Junhua Zhao[1,2*]

Abstract

Carbon nanotube (CNT) networks enable CNTs to be used as building blocks for synthesizing novel advanced materials, thus taking full advantage of the superior properties of individual CNTs. Multiscale analyses have to be adopted to study the load transfer mechanisms of CNT networks from the atomic scale to the macroscopic scale due to the huge computational cost. Among them, fully resolved structural features include the graphitic honeycomb lattice (atomic), inter-tube stacking (nano) and assembly (meso) of CNTs. On an atomic scale, the elastic properties, ultimate stresses, and failure strains of individual CNTs with distinct chiralities and radii are obtained under various loading conditions by molecular mechanics. The dependence of the cohesive energies on spacing distances, crossing angles, size and edge effects between two CNTs is analyzed through continuum modeling in nanoscale. The mesoscale models, which neglect the atomic structures of individual CNTs but retain geometrical information about the shape of CNTs and their assembly into a network, have been developed to study the multi-level mechanism of material deformation and microstructural evolution in CNT networks under stretching, from elastic elongation, strengthening to damage and failure. This paper summarizes the multiscale theories mentioned above, which should provide insight into the optimal assembling of CNT network materials for elevated mechanical performance.

Keywords: Carbon nanotube networks, Hierarchical structures, Multiscale theories, Mesoscale model

1 Introduction

From the stone ages to modern history, new materials have often been the enablers of revolutionary technologies [1]. For a wide variety of envisioned applications in space exploration, artificial muscles, and ballistic armour, materials must be significantly stronger, stiffer, and lighter than those currently available. Carbon nanotubes (CNTs), initially discovered in 1991, have attracted extensive attention by offering extraordinary mechanical properties, including stiffness (~ 1 TPa), strength (~ 120 GPa) and resilience (~ 15% strain to failure) [2–5]. Researchers have been seeking a way to assemble CNTs into the constructed CNT networks, such as fibers [6–10], films [11, 12], and sponges [13, 14] (Figure 1), which can be handled much more conveniently than the individual CNTs. Opposing to CNT arrays in which CNT units are aligned in one direction, CNTs throughout the CNT networks are interconnected with each other. The type of interconnection that dictates the physical properties of the material could be noncovalent (i.e., van der Waals, physical entanglement) or covalent depending on the synthesis method [15–18]. However, the excellent properties of CNTs on the nanoscale have yet to be transferred to these macro-structures due to the inadequate alignment, weak interfacial bonding, and low CNT volume fraction [19, 20].

Many experimental methods have been studied to obtain an oriented microstructure of CNT networks to realize their theoretical properties, including using

*Correspondence: junhua.zhao@163.com

[1] Jiangsu Key Laboratory of Advanced Food Manufacturing Equipment and Technology, Jiangnan University, Wuxi 214122, China
Full list of author information is available at the end of the article

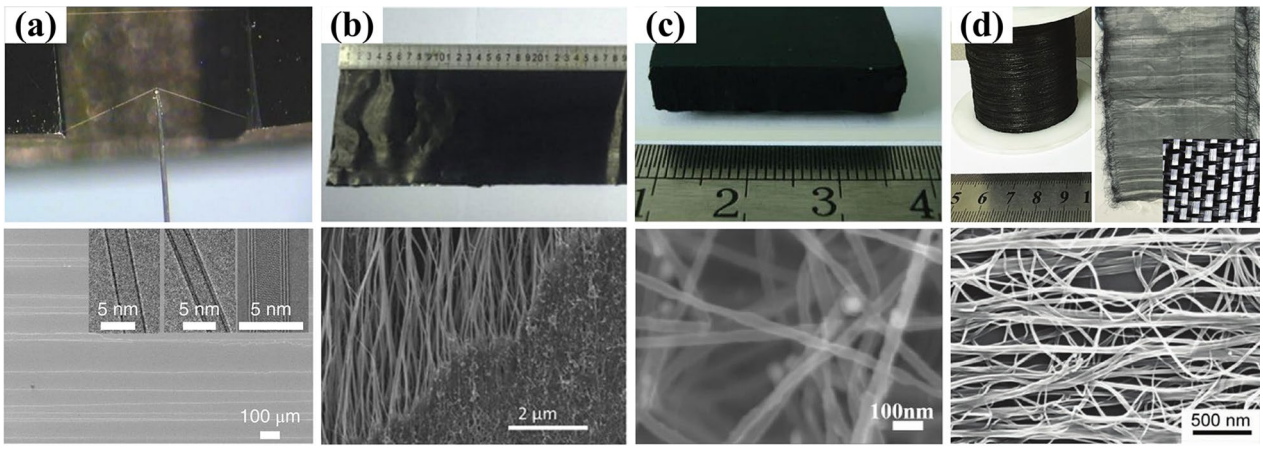

Figure 1 Experimental characterization of four typical constructed CNT networks. SEM images of (**a**) CNT bundles (Inset: high-resolution TEM images of the as-grown ultralong CNTs with single, double and triple walls) [8], (**b**) CNT films [12], (**c**) CNT sponges [13, 14] and (**d**) CNT fibers [9, 10]

plasma enhanced chemical vapor deposition (CVD) to obtain natural growth orientation [21, 22], attempting template/spinning techniques to aid in growth orientation of CNT forests [23, 24], and using magnetic fields to induce alignment [25, 26]. Windle et al. [27] implemented a twisting method that resulted in a tensile strength of 8.8 GPa and Young's modulus of 357 GPa for a CNT fiber with a 1 mm test gauge length. Cheng et al. [28] fabricated CNT sheets with the tensile strength of roughly 2.1 GPa and a modulus of 169 GPa using a mechanical stretching method. Another route to improving the mechanical properties of CNT networks is introducing covalent crosslinks between CNTs which can be induced by the irradiation of CNTs with electron or ion beams [29–31]. It was shown that the crosslinked CNT sheets display improvements in Young's modulus and tensile strength by factors of ~ 3 and ~ 5, respectively [32].

Recently, with the spring up of well-designed microscopy techniques, the hierarchical microstructures of CNT networks were elucidated by providing illustrative views of the multi-level structural units and their interfaces. The nondestructive X-ray scattering was used to quantitatively map the multiscale structure of hierarchically self-organized CNT "forests" across 4 orders of magnitude in length scale, from 2.0 Å to 1.5 μm [33]. The transmission electron microscopy (TEM) and scanning electron microscopy (SEM) studies have shown that the CNT fibers have a multi-scale structure, that is, the fiber itself is on a macroscopic scale, the nanotube bundle and thread on a microscopic scale, and the CNTs on nanoscale [34]. It also has been reported that the CNT films usually feature a porous structure, in which CNTs are randomly distributed and arranged into a nonwoven fibrous structure, as ordinary paper made from wood pulp fibers [11, 35]. Furthermore, the studies by in-situ Raman spectroscopy elucidated the multi-level mechanism of material deformation and microstructural evolution in CNT fibers [36, 37]. TEM analysis of CNT films revealed unusual CNT crystal packing and permitted the observation of interesting structural features of the CNTs and their assemblages, including collapse, flattened packing, preferred stacking, folding and twisting phenomena, as well as CNT pullouts from bundles and the resin matrix [20, 38, 39]. Rate-dependent failure mechanisms were demonstrated for the CNT fibers, with inter-tube slippage occurring at low rates while cascade-like breaking processes dominate at high rates due to the misalignment of CNTs [40–42].

The fundamental understanding of structure-property relationships in hierarchically constructed CNT networks is crucial for the development of new functionality, yet quantifying structure across multiple scales is challenging. Considering the synthetic and assembly procedures, as well as the post-processing techniques, the strength loss of CNT networks compared to defect-free CNTs can be explained by mechanisms including stress localization due to the presence of defects in individual CNTs, insufficient load transfer in closely-packed bundles, and the porous, misaligned bundles in the networks (Figure 2) [43]. Multiscale modelling describes behavior at a given length scale on the basis of the physics at a finer scale, and offers quantitative information about their dimensions that helps in constructing theoretical models to reveal their stretchability and failure mechanism of CNT networks. In the particular case of the microstructural complexity of CNT networks, a breakthrough can be expected when the "bottom-up" manufacturing approach could be used in a controllable and

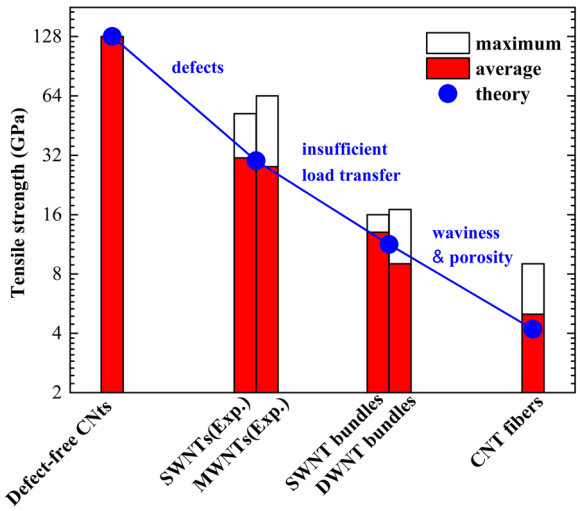

Figure 2 The strength reduction from individual, defect-free CNTs to CNT fibers [43]

self-assembled way, which would favor the fabrication of organized macroscale structures (that is, CNT networks) from nanoscale components.

In this paper, a thorough literature review including recent theoretical and experimental studies is presented, with a focus on the hierarchical structures and mechanical characteristics of CNT network materials. As supporting material, some recent studies will also be introduced to provide insight into modulating the mechanical properties of CNT network materials by designing microstructures. Section 2 summarizes the elastic properties, ultimate stress, and failure strain of individual CNTs under various loading conditions and special attention has been paid to the effects of the tube chirality and tube size. Section 3 describes the cohesive energy and the equilibrium distance for two parallel CNTs, two crossing CNTs and CNT/substrate based on the continuum models of van der Waals interactions between them. In Section 4, the mesoscale models for CNTs are presented, which can be used to efficiently characterize the nonlinear mechanical behaviors and understand the failure mechanism of the CNT networks. The conclusions are drawn in Section 5.

2 The Mechanical Behaviors of Individual CNTs

Many experimental studies gave direct proof of the exceptional mechanical properties of CNTs. By investigating vibration frequencies of cantilevered CNTs by the TEM technology, Treacy et al. [44] obtained Young's modulus of CNTs in the range from 0.4 to 4.15 TPa, with a mean value of 1.8 TPa. Yu et al. [45] directly applied axial tensile force on both ends of a CNT using an atomic-force microscope, and measured Young modulus ranging from 0.27 to 0.97 TPa and the ultimate strength of the outmost layer varying from 11 to 63 GPa. Theoretical studies could provide more detailed information than experimental investigations. Two alternative approaches, namely the "top-down" approach based on continuum mechanics and the "bottom-up" approach based on molecular mechanics, are frequently used to model the mechanical properties of nano-structured materials. Yakobson et al. [3] studied the buckling of CNTs under axial compression, bending and torsion and showed that the buckling behavior of a CNT can be well predicted by a continuum shell mode. Ru [46, 47] proposed that the effective bending stiffness of nanotubes should be regarded as an independent material parameter not related to the representative thickness by the classic bending stiffness formula. Zheng et al. [48] obtained Young's modulus of CNTs by measuring resonance frequency and using the modulus-frequency relation resulting from the linear vibration theory. The Young's modulus decreases sharply, from about 1 to 0.1 TPa with the diameter increasing from 8 to 40 nm, and the investigators attributed this decrease to the emergence of an unusual bending mode during the measurement that corresponds to rippling on the inner arc of the bent nanotubes. Wang et al. [49] concluded that the thin-shell model of SWNTs has helped to reproduce many complex mechanical phenomena of CNTs observed in experiments, such as buckling of single-walled CNT, unstable behavior or phase transformations of single-walled CNT bundles, and bending and torsional ripples of multi-walled CNTs, and may guide to create new structural materials that have unusual or multifunctional properties. Li et al. [50, 51] developed a beam model of CNTs which assumes that the beam elements have circular cross sections and are always subjected to pure tension, pure bending, and pure torsion. Kasti [52] found that the beam bending stiffness BBS (EI/b, where E is Young's modulus, b is the beam length, and I is the moment of inertia of the beam) is equal to the bond bending stiffness of zigzag CNTs. However, it is difficult to account for the possible effect of tube chirality on the behavior of CNTs in a continuum mechanics model because the discrete nature of atomic structures is merged.

Recently, molecular mechanics has been used to obtain closed-form solutions for the elastic properties of CNTs. A truss model was presented by Odegard et al. [53] to establish the relationship between effective bending rigidity and molecular properties of a graphene sheet by equating the molecular potential energy to the mechanical strain energy. Chang et al. [54–56] established a "stick-spiral" model (SSM) which is capable of predicting not only the initial elastic properties (e.g.,

Young's modulus) but also the stress-strain relations of a CNT under axial, radial, and torsion conditions. In this model, a stick with infinite bending stiffness is used to model the force-stretch relationship of carbon-carbon bond, and a spiral spring is used to describe the twisting moment resulting from an angular distortion of the bond angle. Zhao et al. [57, 58] showed that the two molecular mechanics models, the beam and SSM models, predict considerably different mechanical properties of materials based on energy equivalence. Comparing the two models with the molecular dynamics (MD) results, it could be found that the SSM model overestimates and the beam model underestimates the mechanical properties of CNTs under pure bending conditions.

Favata et al. [59] first proposed a nonlinear discrete mechanical model to predict the natural equilibrium radius of a chiral CNT (armchair or zigzag) by considering the CNT geometry and the prestress state based on the Reactive Empirical Bond-Order interatomic potential (REBO potential) of the second generation. Note that the REBO potential is extensively taken as the most accurate potential to characterize the mechanical properties of CNTs [60]. Considering an (n, m) CNT subjected to an axial force F (Figure 3), the nonlinear SSM model based on the REBO potential can then be established according to the geometrical relationships, the moment equilibrium equations, and the compatible equation for a deformed CNT. Figure 4(a) and (b) shows the stress-strain curves and energy-strain curves of different chiral CNTs under tension and compression (before buckling) based on the REBO potential using the SSM [61]. It can be found that the present results of the nonlinear SSM agree well with those of full-atom MD simulations. The nonlinear mechanical properties, especially the ultimate strains and stresses, strongly depend on the CNT chirality but weakly depend on CNT radii. When a CNT radius R > 6 Å, both ultimate strains and ultimate stresses are both independent of the CNT radius, as shown in Figure 4(c). The chirality-dependent ultimate strains and stresses (R > 6 Å) as well as their data fitting are shown in Figure 4(d), in which the hollow circles and boxes represent the ultimate stresses and strains of the corresponding single-layer graphene sheets with different chirality, respectively.

The bending behavior of a CNT from the SSM based on the REBO potentials was further studied in Ref. [61]. The upper part of the CNT under pure bending loading is subjected to the tensile force while the lower part is subjected to the compressive force, as shown in Figure 5(a). Based on the SSM, the axial forces of f_{1i} and f_{2i} can be expressed as

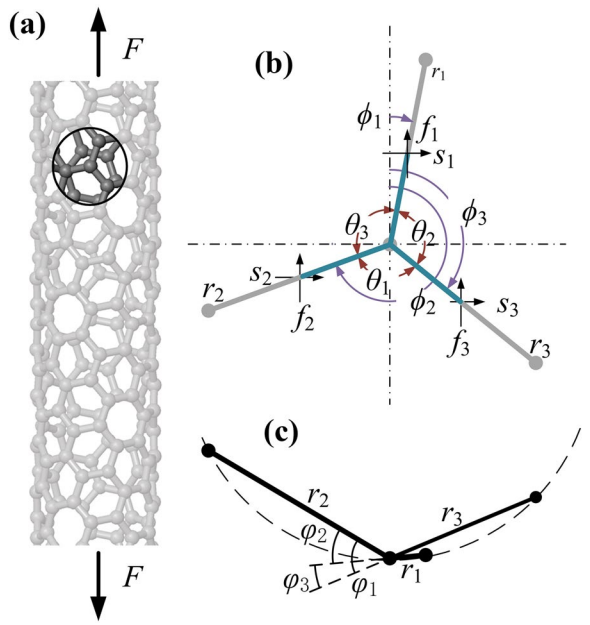

Figure 3 The geometric parameters of a chiral CNT in the stick-spiral model [56]: (**a**) global structure, (**b**) front view and (**c**) top view of local structure

$$F_{1i} = F_1[\varepsilon_i] = F_1\left[\varepsilon' \cos\left(\frac{i \cdot 360^\circ}{n+m}\right)\right], \tag{1}$$

$$F_{2j} = F_2[\varepsilon_j] = F_2\left[\varepsilon' \cos\left(\frac{j \cdot 360^\circ - 180^\circ}{m}\right)\right], \tag{2}$$

where $i = 1, 2, \ldots, n+m$, and $j = 1, 2, \ldots, m$. Both n and m are the chiral parameters of the CNT. ε' is the maximum tensile strain of the CNT under bending loading. $F_1(\varepsilon)$ and $F_2(\varepsilon)$ are the function between the axial strain and the axial force of the two types bonds in CNTs, respectively. To obtain the M (total bending moment of the CNT), the bending moments of all cross-sectional bonds can be summed as

$$M = R \cdot \left[\begin{array}{l} \sum_{i=1}^{n+m} f_{1i} \cdot \cos\left(\frac{i \cdot 360^\circ}{n+m}\right) + \\ \sum_{j=1}^{m} f_{2j} \cdot \cos\left(\frac{j \cdot 360^\circ - 180^\circ}{m}\right) \end{array}\right]. \tag{3}$$

Figure 5(b) shows the bending behavior of CNTs under pure bending using the SSM and MD simulations. The difference between the SSM and beam model decreases with increasing CNT radii. Figure 5(c) shows the distribution of bending moments for different (5, 5) CNT lengths L with bending angle using MD simulations

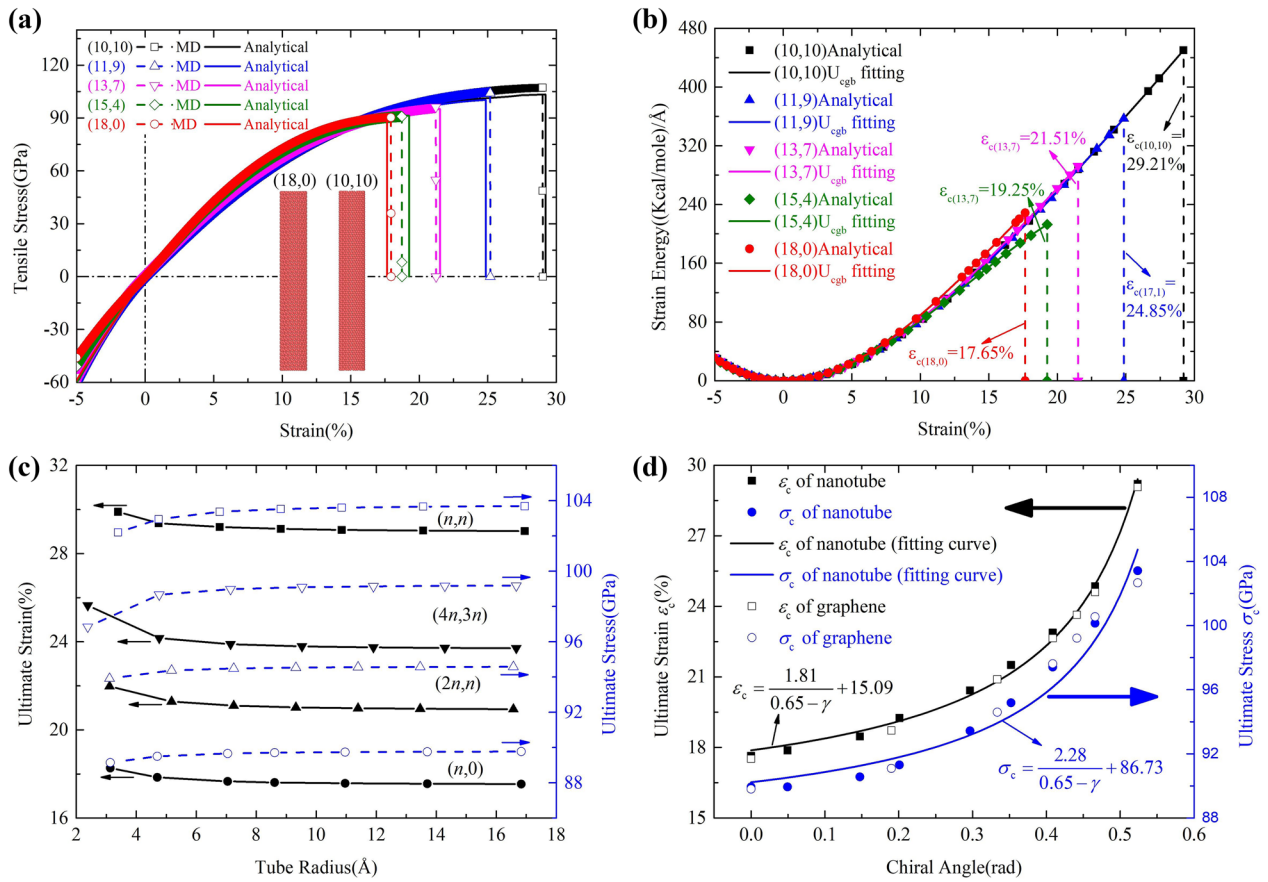

Figure 4 The mechanical properties of different chiral CNTs [61]: (**a**) The stress-strain curves of CNTs, (**b**) The strain energy vs strain curves per unit length of CNTs. The distribution of ultimate strains and stresses with (**c**) CNT radii for different chiral CNTs and (**d**) CNT chirality for a given CNT radius (around 6.8 Å)

based on the REBO potential. Afterwards, the distribution of the bending energy per unit length for different chiral CNTs with bending angle using the SSM and MD simulations based on the REBO potential, where the lengths of the chiral CNTs are chosen as in the range of 8–10 nm, as shown in Figure 5(d). The bending moments of different chiral CNTs using MD simulations are close to those using the SSM.

Recently, CNTs filled with linear mass chains (such as carbon-atom chains) have received much attention because of their potential applications in nanoelectronic devices. It is well-known that the vdW interactions between the filled mass chain and the CNT play a significant role in the dynamic behaviors of such CNT composite structures. Ding et al. [62] obtained closed-form expressions for the vibration of the carbon-atom chain inside the CNT based on the continuum modeling of the vdW interactions between the carbon-atom chain and the CNT (Figure 6(a)). Meanwhile, the effect of the initial tensile force, the amplitude of the carbon chain, and the radii of the CNTs on the vibration frequency were also studied in detail, where all theoretical results were validated by MD simulations reasonably. Then, Liu et al. [63] presented a detailed study on the propagation characteristics of terahertz (THz) flexural wave propagation in mass chain-filled CNTs using a continuum mechanics approach and MD simulations (Figure 6(b)). In this study, the effect of the surrounding elastic medium and the vdW interactions between the CNT and the filled mass chain on the wave frequency was considered, and the results showed that the wave propagation of a CNT could be modulated by changing the filled mass chain and the surrounding elastic medium. To design and manufacture reliable nanoelectronic devices in the future, the mechanical properties of CNTs filled with linear carbon-atom chains were also a critical issue and should be studied in detail. Zhu et al. [64] investigated the buckling behaviors of such CNT composite structures under torsion, bending, and compression using MD simulations (Figure 6(c) and (d)). Meanwhile, they considered the effect of the

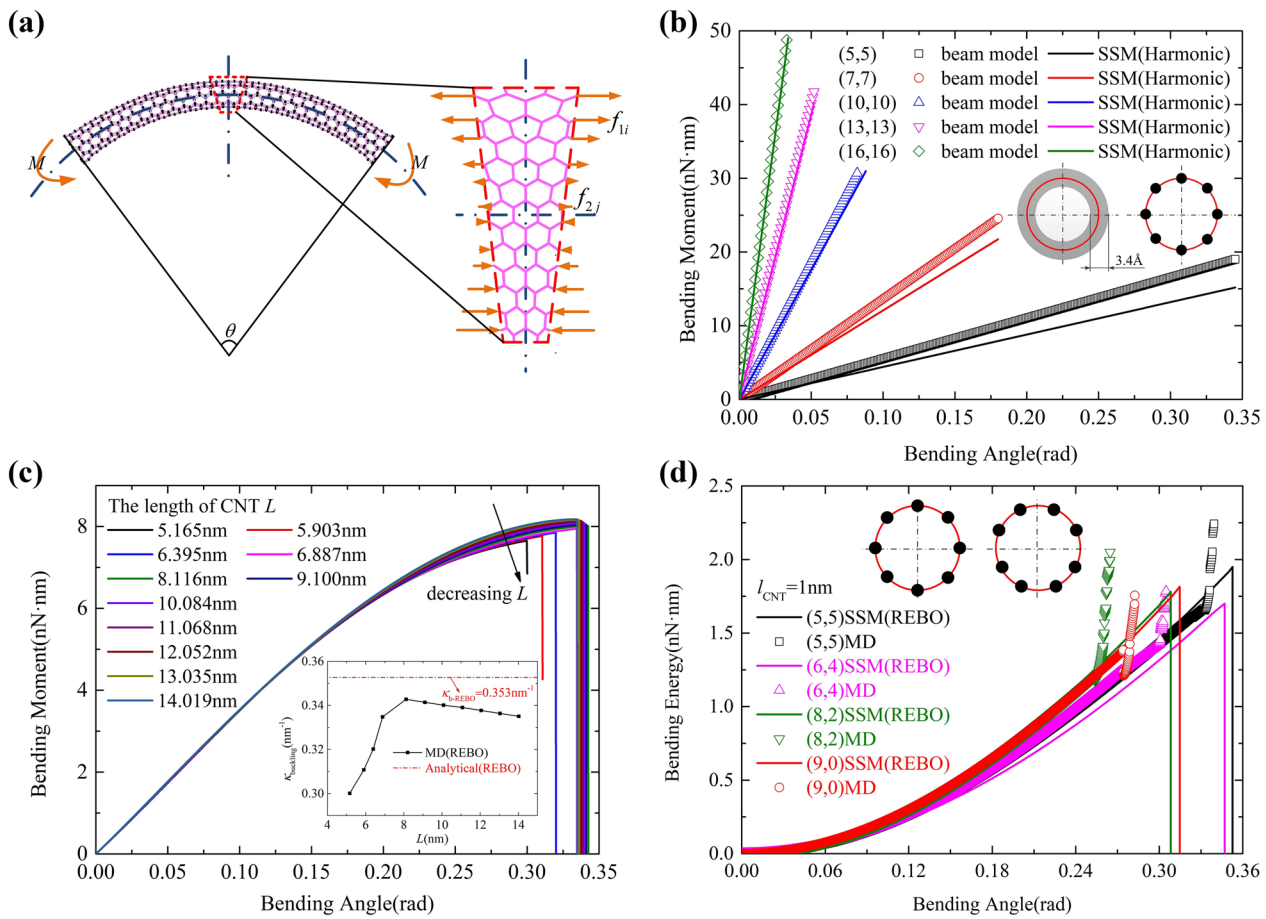

Figure 5 The bending behaviors of CNTs [61]: (**a**) Schematic diagram of a CNT under bending, (**b**) The distribution of bending moment for different CNT radii with bending angle, (**c**) The distribution of bending moment for different CNT lengths with bending angle, and the inset represents the critical buckling curvature with *L*, (**d**) The distribution of the bending energy per unit length for different chiral CNTs with bending angle

length and chirality on buckling, and found that the buckling improvement was not obvious for a short-filled CNT because the radial vdW force between the carbon-atom chain and the CNT was very small.

3 The Interface Properties of CNTs in CNT Networks

As mechanical structures enter the nanoscale regime, the vdW interaction plays a significant role. It has been well established that the mechanical behavior of CNTs is also strongly influenced by the vdW force [65–67]. A good understanding of the vdW interactions for two crossing CNTs, CNT/graphene, and CNT/substrate is essential to ensure the optimum performance of CNTs in potential applications.

Zhao et al. [68, 69] obtained the closed-form expressions on the cohesive energy and the equilibrium distances between the two parallel CNTs and two crossing CNTs from a continuum model based on the Lennard-Jones (LJ) potential. The energy of the vdW interactions between two carbon atoms of the CNTs was given by

$$V(d) = 4\varepsilon_{\mathrm{c-c}}\left[\left(\frac{\sigma_{\mathrm{c-c}}}{d}\right)^{12} - \left(\frac{\sigma_{\mathrm{c-c}}}{d}\right)^{6}\right], \tag{4}$$

where d is the distance between the interacting atoms, $\varepsilon_{\mathrm{c-c}}$ is the depth of the potential, $\sigma_{\mathrm{c-c}}$ is a parameter that is determined by the equilibrium distance ($\varepsilon_{\mathrm{c-c}} = 2.8437$ meV and $\sigma_{\mathrm{c-c}} = 3.4$ Å are adopted from the literatures). Figure 7(a) shows the coordinate system and a schematic diagram of the two parallel infinite CNTs. The upper and lower CNT radii are r_1 and r_2, respectively. The closest distance between the two parallel CNTs edge is h. From the geometry, the energy per unit length along the z direction on the lower CNT from the vdW interactions can be obtained as

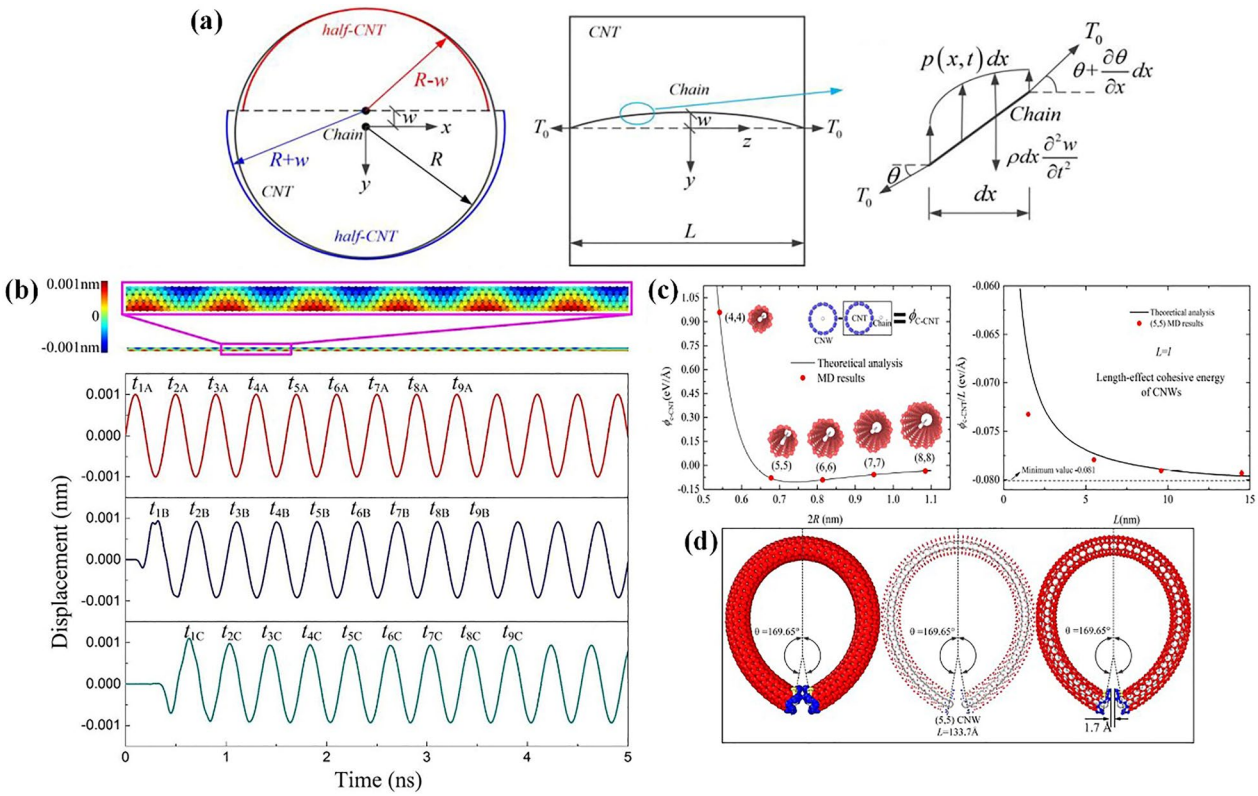

Figure 6 (**a**) Schematic diagrams of CNTs filled with linear mass chains [62], (**b**) MD simulations of flexural wave propagation in a carbon-atom chain-filled CNT [63], (**c**) The cohesive energy and (**d**) bending behaviors of infinite filled CNTs [64]

$$\phi_{\text{cicle}} = \int_0^{2\pi} \rho r_2 \mathrm{d}\theta_2 \int_{-\infty}^{\infty} V(d)\mathrm{d}z \int_0^{2\pi} r_1 \mathrm{d}\theta, \tag{5}$$

where ρ is the area density, and can be expressed as $\rho = 4/(3\sqrt{3}b^2)$, where $b = 1.42$ Å is the bond length of CNTs. Figure 7(c) compares the cohesive energy for different distances between the two parallel infinite CNTs (where $r_1 = r_2$) from this analytical model with results from MD simulations. The cohesive energy increases with decreasing CNT radius. Similarly, the crossing angle between the two center axes of the two crossing CNTs is denoted as β ($0 < \beta \leq 90°$) (Figure 7(b)). Since the cohesive energy on each CNT circle per unit length is nonuniform, the total cohesive energy of the two CNTs due to the vdW force can be written as

$$\phi_{\text{total}} = \int_0^{2\pi} \rho r_2 \mathrm{d}\theta_2 \int_{-\infty}^{\infty} 1\mathrm{d}z_2 \int_{-\infty}^{\infty} V(d)\mathrm{d}z \int_0^{2\pi} r_1 \mathrm{d}\theta. \tag{6}$$

Figure 7(d) shows the distribution of cohesive energy with different distances between two crossing infinite CNTs at $\beta = 90°$ using this present analytical model and MD simulations. Interestingly, the equilibrium distance between two crossing CNTs is independent of β. The results from Eqs. (5) and (6) agree well with the results from the MD simulation [68].

Explicit expressions for the size- and edge-effect cohesive energy between two finite-sized CNTs were further obtained through continuum modeling of vdW interactions between them [70]. The close-form solutions of the cohesive energy ϕ_{total} between these structures at different positions were derived using Gaussian quadrature, and then the average cohesive energy per unit length along the central axis of CNT could be obtained as $\phi_{\text{ave}} = \phi_{\text{total}}/L$, where L is the length of CNTs. The size-effect cohesive energy between two parallel finite CNTs from the present analytical model is shown in Figure 8(a) and (b). For given radii of two parallel CNTs, ϕ_{ave} tends to have different constants when the length of CNTs is higher than 10 nm, which indicates that the size effect of the cohesive energies for different radii of CNTs can be neglected as $L > 10$ nm. Moreover, the shear cohesive stress was obtained as $\tau_{\text{cohesive}} = \partial\phi_{\text{ave}}/\partial a$, where a is the lateral distance between the two CNTs. The two lengths of the upper and lower CNTs (5, 5) are around 30 Å and 10 Å, respectively. Figure 8(c) shows the comparison of the average cohesive energy by considering the edge

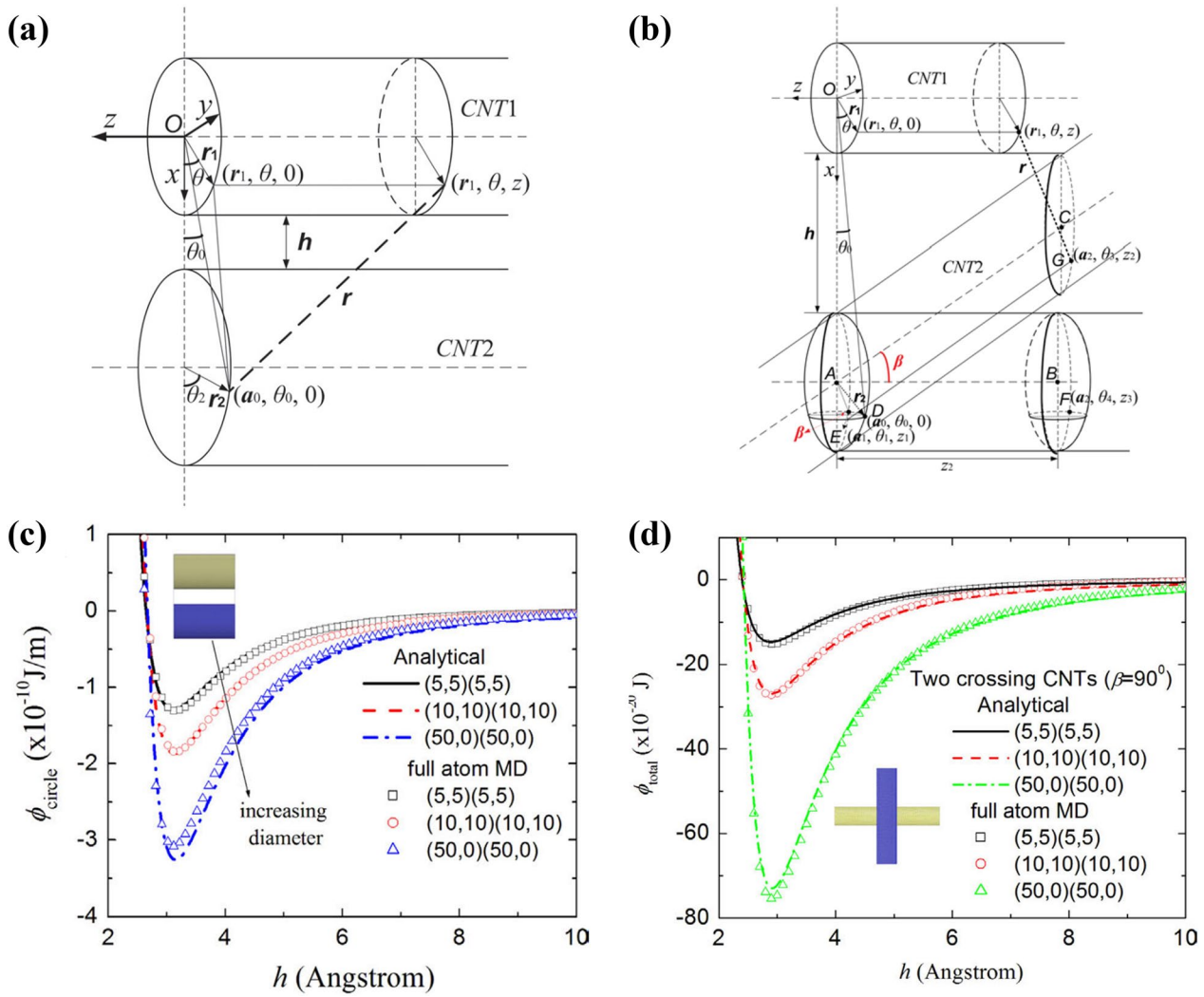

Figure 7 The coordinate system of (**a**) the two parallel infinite CNTs and (**b**) the two crossing infinite CNTs. The distribution of cohesive energy with different distance between (**c**) two parallel infinite CNTs and (**d**) two crossing infinite CNTs [68]

effect or not. The edge effect on the cohesive energy is remarkable when the right boundary of the lower CNT is close to overlapping the upper CNT along the x direction. Figure 8(d) shows the distribution of the cohesive shear stress with a. One can find that both the maximum repulsive and attractive shear stresses are always close to the initial intersecting positions between them.

Recently, Geblinger et al. [71] reported the experimental and molecular dynamics realization of S-like shaped single-walled CNTs, the so-called CNT serpentines. Zhao et al. [72] reported results from continuum modeling of the binding energy between different CNTs serpentines and substrates as well as the mechanical stability of the CNT serpentine formation (Figure 9(a)). It is found that the critical length for the mechanical stability and adhesion of different CNT serpentines was determined in dependence on the CNT bending stiffness and distance of the CNT translation period.

It should be noted that the cohesive energy and shear stress mentioned above were obtained from the continuum modeling by homogenizing the carbon atoms on a shell model and representing them by an area density ρ. However, the effect of atomic lattice would play an important role in parallel CNTs of commensurate. Li et al. [73] studied the interfacial shear strengths or static frictions between CNTs in contact at different cross angles using atomic mechanics. It was shown that the axial interfacial shear strengths between parallel CNTs in commensurate are two orders of magnitude greater than those in incommensurate. In contrast, the interfacial

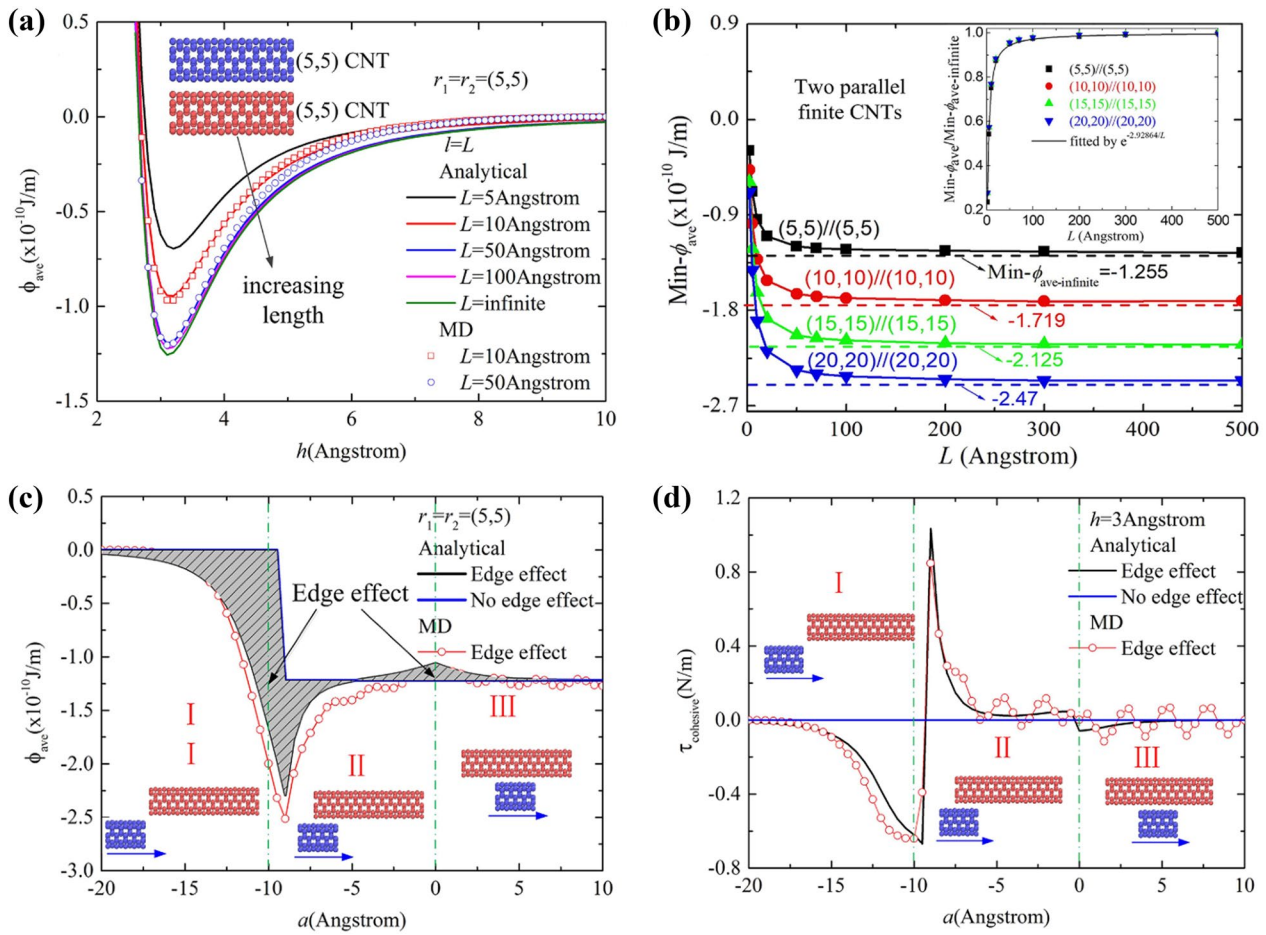

Figure 8 Size-effect and edge-effect cohesive energy between two parallel finite CNTs [70]: (**a**) The distribution of average cohesive energy between two parallel finite CNTs with different vertical distance *h*, (**b**) The distribution of the minimum average cohesive energy Min-φ_{ave} between two (5,5) CNTs with different length *L* (inset represents the normalized Min-φ_{ave}). The distribution of (**c**) the average cohesive energy and (**d**) the shear stress with different lateral distance *a*

shear strengths of crossly contacted CNT pairs are much less dependent upon chirality.

Moreover, the thermo-mechanical vibration of a CNT on a substrate was studied using a nonlocal elastic plate model and two nonlocal elastic beam models (including the Timoshenko-beam model and Euler-beam model) with quantum effects, respectively (Figure 9(b)) [74]. The effect of the vdW interactions between the CNT and the substrate on the vibration was obtained. In particular, the radial vibration of the CNT on the substrate with quantum effects was further derived through the continuum shell model due to the different vdW forces on each point of the CNT circumference. The present models showed that the normalized transverse frequency decreases and the normalized radial frequency increases with increasing CNT radius, respectively. The radial amplitude of the CNT nonlinearly increases and the transverse amplitude of the CNT linearly increases with increasing temperature for a given distance, respectively. The peeling behavior of CNTs from a substrate was studied using the Kendall model of the continuum mechanics, where the elastic CNT with the closest distance is attached to a rigid surface and then subjected to a peeling force at an inclined angle. (Figure 9(c)) [75]. The analytical results showed that the peeling behavior strongly depends on the peeling angle, the pre-tension, the separation distance toward the substrate, the radius, and Young's modulus of the CNT. Dong et al. [76] developed a refined beam model to describe the buckling characteristics of hollow metal nanowires encapsulating CNTs (NWs@CNTs), where the interfacial vdW interaction, interfacial shear stress as well as surface effect are taken into consideration (Figure 9(d)). The analytical expressions for cohesive energies of the vdW interaction between CNTs and hollow nanowires were obtained through continuum modeling. The interfacial shear coefficients for NWs@CNTs

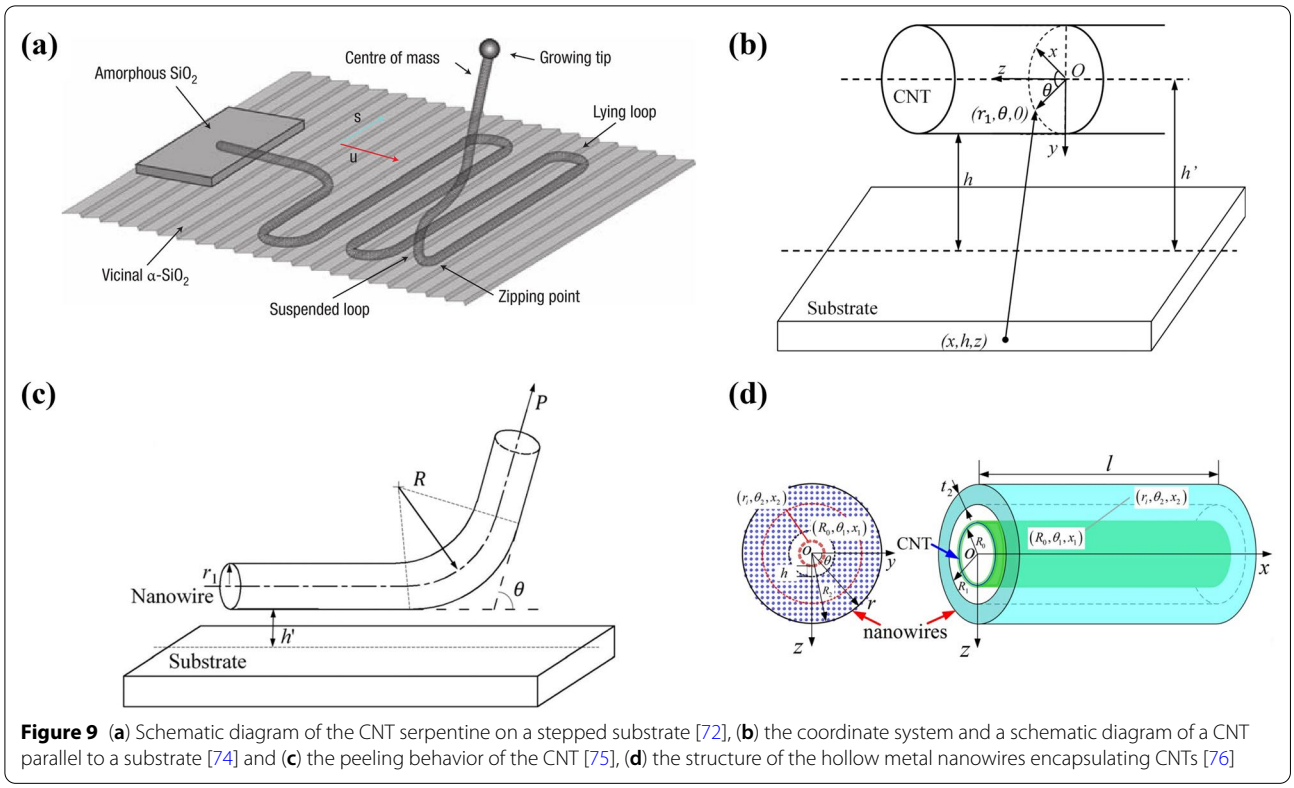

Figure 9 (**a**) Schematic diagram of the CNT serpentine on a stepped substrate [72], (**b**) the coordinate system and a schematic diagram of a CNT parallel to a substrate [74] and (**c**) the peeling behavior of the CNT [75], (**d**) the structure of the hollow metal nanowires encapsulating CNTs [76]

with CNTs of different diameters and nanowires of different lattice orientations were derived by the MD simulations. The surface effects of nanowires were addressed by a function of the bulk surface energy density and surface relaxation parameter. This study could provide theoretical support to prepare vertically aligned CNT arrays with nanoscale conformal coatings and to understand the stability and reliability of CNT reinforced composites.

4 The Mesoscale Model for CNT Networks

Following a maturation period that builds up more information on the physical and chemical characteristics of individual CNTs, in the last decade, network-type materials consisting of CNTs have emerged extending spatial functionalities of individual CNTs to the microscales and macroscales. Through the synthesis of CNT network materials, limitations on capitalizing the superior properties of individual CNTs are being overcome, and the scope of applications is being widened. However, mostly based on the experimental efforts, researchers have noted that the mechanical properties of CNT-based network materials can differ from the individual CNTs significantly depending on the network morphology and characteristics of the CNT interactions within the network. As the deformation develops under applied loads, the local structure of the network is also reorganized, which in turn modifies the mechanical properties of the network interactively. From the point of engineering, it is significant and necessary to quantitatively understand the structure-property relationship and failure mechanism of the CNT networks. Full-atom MD simulations are widely applied to study the mechanical behavior of CNTs and have proven to be a useful approach. However, due to the huge computational cost, such models are limited to very short time- and length-scales so a direct comparison with experimental scales is often extremely difficult or impossible.

To overcome those limitations, a mesoscale model for CNTs was first developed by Zhigilei et al. [77] based on a coarse-grained (CG) representation of CNTs as "breathing flexible cylinders" consisting of a variable number of segments. This mesoscopic model was shown to reproduce well the dynamic behavior of individual CNTs predicted in atomic simulations, but ignores the cohesive energy between CNTs. Buehler et al. [78, 79] were among the first who developed a mesoscale model to investigate the non-bonded CG potentials of the interaction between CNTs, where CNTs are represented as a collection of beads connected by spring-like molecular multi-body interatomic potentials. These interaction potentials describe the resistance to tensile load, bending, and interaction between different CNTs, with parameters rigorously derived from full-atom MD simulations. The mesoscale model is capable of treating the deformation

physics of large assemblies of CNTs corresponding to systems with millions of atoms while incorporating nonlinear elasticity, fracture behavior, and adhesion properties between different CNTs, ranging through time scales of several microseconds. The CG model for CNTs was further developed by Zhao et al. [80, 81]. Based on the analytical results of the cohesive energy between two parallel and crossing CNTs, the non-bonded CG potentials between different CG beads are systematically analyzed.

By combining the bonded potentials with non-bonded potentials, the CG model applies to large deformations of complex CNT systems. Taking into account the stochastic nature of CNT networks, structural evolution and corresponding effects on the mechanical performance of noncovalent 2D CNT network materials have been investigated through CG MD simulations [82, 83]. According to that, in the initial phase of the tensile loading, an affine deformation character was recognized, which was explained by the local stretching of vdW binding sites. Under large strain, the deformation character turned into nonaffine deformation due to the bundling process of CNTs. After a detailed discussion about the microstructural evolution and its effects on mechanical behavior, they concluded that the mechanical properties of CNT networks could be improved by avoiding inter-tube sliding and enhancing the network deformation affinity.

The mechanical enhancement of CNT networks by mobile and discrete binders was then explored by Wang et al. [84, 85]. Using CG MD simulations, they performed tensile tests and dynamical mechanical analysis (DMA) to quantify the strength, energy dissipation capacity, and viscoelastic performance of the material. Simulation results showed that binders are apt to aggregate and cluster at the junctions between CNTs, resisting the reorientation, bundling, and sliding processes that lead to the microstructural evolution of the network. The effects enhance the strength, energy dissipation capacity and storage modulus of the network generally. Yang et al. [86] employed the CG MD simulations to investigate the nonlinear large-deformation behavior and the fracture mode of crosslinked CNT networks by considering both intrinsic intra- and inter-tube bond-breaking. A critical crosslink density ρ_c was found to divide the deformation mode of CNT networks into two regimes in uniaxial tension, i.e., the bending-dominated mode at $\rho < \rho_c$ and the bending-stretching-bending three-stage one at $\rho > \rho_c$. This transition is attributed to the stress concentration and the intrinsic bond-breaking in large tensile deformations. Meanwhile, the effects of the CNT length and material structure on the mechanical properties of free-standing thin CNT films with continuous networks of bundles of nanotubes and covalent crosslinks were studied by Volkov et al. [87, 88]. It was found that the tensile modulus and strength of the CNT films strongly increase with increasing CNT length, but the effect of the nanotube length is altered by the crosslink density. The dispersion of nanotubes without formation of thick bundles results in a few-fold increase in the modulus and strength. The variation of the film properties was explained by the effects of the CNT length, crosslink density, and network morphology on the network connectivity. Chen et al. [89, 90] studied the change in stiffness of the CNT networks and revealed the existence of a stiffness threshold. Two critical network densities were found to divide the stiffness behavior into three stages: zero stiffness, bending-dominated and stretching-dominated stages. The first critical network density is a criterion to judge whether or not the network is capable of carrying the load, defined as the stiffness threshold. The second critical network density is a criterion to measure whether or not most of the CNTs in the network are utilized effectively to carry the load, defined as bending–stretching transitional threshold.

The electrical resistance of a thin CNT film has been widely found to increase with increasing strain but remains almost constant as strain is released, forming a hysteresis between loading and unloading. However, the understanding of the microstructural origin of this strain dependence is a big challenge. Jin et al. [91] investigated the relationship among the loading and unloading cycles, the network morphological evolution, and the resistance change via CG molecular statics simulations, analytic modeling, and experiments. It is found that the hysteretic resistance–strain behavior of the CNT films is controlled by the microstructure parameter ξ, the mean relative projected length of CNTs. The decrease of ξ during loading is caused by the combination of CNT reorientation and sliding, and the tendency for long CNTs to buckle causes ξ to stay nearly constant during unloading. In the limit of high contact resistance, the electrical resistance of the film is proportional to ξ^{-2}, where ξ acts as a "mean free path" relative to the film dimension along which the charge can travel without experiencing Ohmic loss at the CNT contacts. The findings are generally applicable to any stretchable thin film conductors consisting of 1D conductors with much lower resistance than the contact resistance in the high-density regime.

In a more recent study, Ji et al. [61] completely established the explicit expressions of the chirality-dependent higher-order nonlinear CG stretching and bending potentials based on the REBO potential (Figure 10). The total energy, U_{cg} of a CNT was written as the sum of energies associated with the variance of the CG bond length U_{cgb}, and the CG bond angle, $U_{cg\theta}$, i.e.

$$U_{cg} = U_{cgb} + U_{cg\theta}. \tag{7}$$

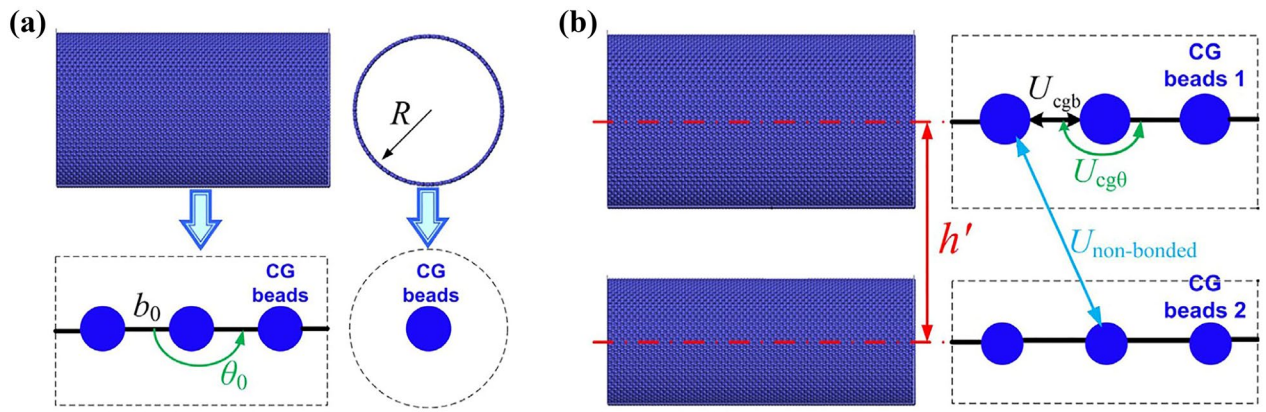

Figure 10 Two parallel CNTs and their CG model. The full-atom atomic structure and CG model for (**a**) a CNT and (**b**) two parallel CNTs

The high-order nonlinear expressions of U_{cgb} can be written as

$$U_{cgb} = \sum_i \begin{bmatrix} K_{cgb2}(db_{cgi})^2 + \\ K_{cgb3}(db_{cgi})^3 + K_{cgb4}(db_{cgi})^4 \end{bmatrix}, \quad (8)$$

where db_{cgi} is the bond elongation of CG bond i. K_{cgb2}, K_{cgb3}, K_{cgb4}, are force constants, and can be derived by data fitting for the nonlinear stress-strain curves of different chiral CNTs (Figure 4). It is interesting to find that a good linear relationship is always met between the three constants and CNT radii R. Therefore, the three constants can be expressed as

$$\begin{cases} K_{cgb2} = a_{cgb2} \cdot R, \\ K_{cgb3} = a_{cgb3} \cdot R, \\ K_{cgb4} = a_{cgb4} \cdot R, \end{cases} \quad (9)$$

where a_{cgb2}, a_{cgb3} and a_{cgb4} are the functions of the CNT chiral angle (γ), respectively. Based on the present analytical results, K_{cgb2}, K_{cgb3}, and K_{cgb4} were fitted as a_{cgb2}=319 (Kcal/mole)/Å^3, $a_{cgb3} = 118.51\gamma^2 - 118.51\gamma - 127.89$ (Kcal/mole)/Å^4, and $a_{cgb4} = -109.97\gamma^2 + 113.31\gamma + 5.37$ (Kcal/mole)/Å^5. Similarly, the higher-order nonlinear expressions of $U_{cg\theta}$ can be written as

$$U_{cg\theta} = \sum_j \begin{bmatrix} K_{cg\theta2}(d\theta_{cgj})^2 + \\ K_{cg\theta3}(d\theta_{cgj})^3 + K_{cg\theta4}(d\theta_{cgj})^4 \end{bmatrix}, \quad (10)$$

where $d\theta_{cgj}$ is the variance of the CG bond angle j. The three force constants ($K_{cg\theta2}$, $K_{cg\theta3}$, $K_{cg\theta4}$) were obtained by fitting the bending energy versus the bending angle curve of the CNT before buckling. It should be noted that the bending behavior of all CNT radii under pure bending is almost linear (Figure 5). Therefore, the three constants of CG bending potentials with CNT radii and CNT chiral angle can be expressed as

$$\begin{cases} K_{cg\theta2} = a_{cg\theta2} \cdot R^3, \\ K_{cg\theta3} = 0, \\ K_{cg\theta4} = 0, \end{cases} \quad (11)$$

where $a_{cg\theta2}$ is the function of the CNT chiral angles, and was fitted as $a_{cg\theta2} = -0.285\gamma^2 - 0.042\gamma + 1.044$ nN·nm^{-2}.

To obtain the non-bonded CG potentials, the cohesive energy between two parallel CNTs or two crossing CNTs was described by two parallel CG bead chains or two crossing CG bead chains, where the CG beads chains can be also taken as two corresponding lines [61]. The cohesive energy per unit length of two parallel lines can be expressed as

$$\phi_{line\text{-}line} = \rho_1^2 \int_{-\infty}^{\infty} V(d)\mathrm{d}x, \quad (12)$$

where, d=x+h', ρ_1 is the line density, h' is the distance between the two lines. $V(d)$ is the function of vdW interactions between the CG beads, which can be described by LJ potentials (such as 6–9 LJ, 18–24 LJ potential or other forms). Considering the form of 18–24 LJ potential, the $V(d)$ was expressed as

$$V_{18-24}(d) = \frac{256}{27}\varepsilon_{18-24}\left[\left(\frac{\sigma_{18-24}}{d}\right)^{24} - \left(\frac{\sigma_{18-24}}{d}\right)^{18}\right], \quad (13)$$

where $\varepsilon_{18\text{-}24}$ is the depth of the potential, and $\sigma_{18\text{-}24}$ is the parameter that is determined by the equilibrium distance between the two CG beads on two different CG bead chains. The $\phi_{line\text{-}line}$ was used to fit the cohesive energy

between CNTs based on the full-atom results (Eqs. (5) and (6)), and then the parameters of $V(d)$ can be derived. It is found that a higher-order LJ potential can be used to describe the cohesive energy more accurately, such as the 18–24 LJ potential (Figure 11). All values of $\varepsilon_{18\text{-}24}$ and $\sigma_{18\text{-}24}$ for chiral CNTs are obtained based on the fitting results [61].

The nonlinear mechanical behaviors for a (10, 0) CNT under transverse energy were obtained by the full-atom and CG MD simulations (Figure 12(a)) [61]. The CG MD results were in good agreement with those of full-atom MD simulations, in which much lower computational cost is needed. To compare the computational cost between the full-atom and CG MD simulations, Figure 12(b) shows the change in the computational time of (10,0) CNT with different lengths of the CNT (L_0) under transverse tension using two kinds of MD methods. For a given L_0, the computational cost of CG MD simulations is around 2–5 orders of magnitude reduction by comparison with that of full-atom MD simulations.

CNT bundles are a set of aligned tubes arranged in a 2D triangular lattice in the plane perpendicular to their common axes and are considered one of the strongest fiber materials. The first experimental value of shear moduli of the CNT bundle was given by Salvetat et al. [92]. It is about the out-of-plane shear moduli c_{44}, with values of 0.7–6.5 GPa (±50%), estimated from the force-deflection measurements of CNT bundles as suspended beams loaded by atomic force microscopy (AFM). Saether et al. [93] calculated the area modulus, shear modulus, Young's

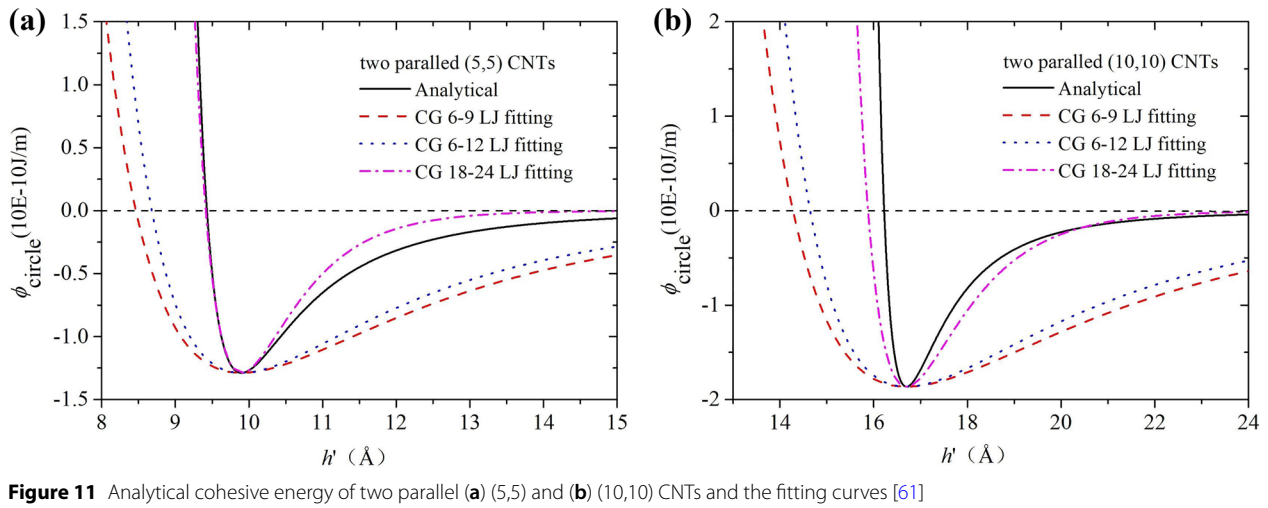

Figure 11 Analytical cohesive energy of two parallel (**a**) (5,5) and (**b**) (10,10) CNTs and the fitting curves [61]

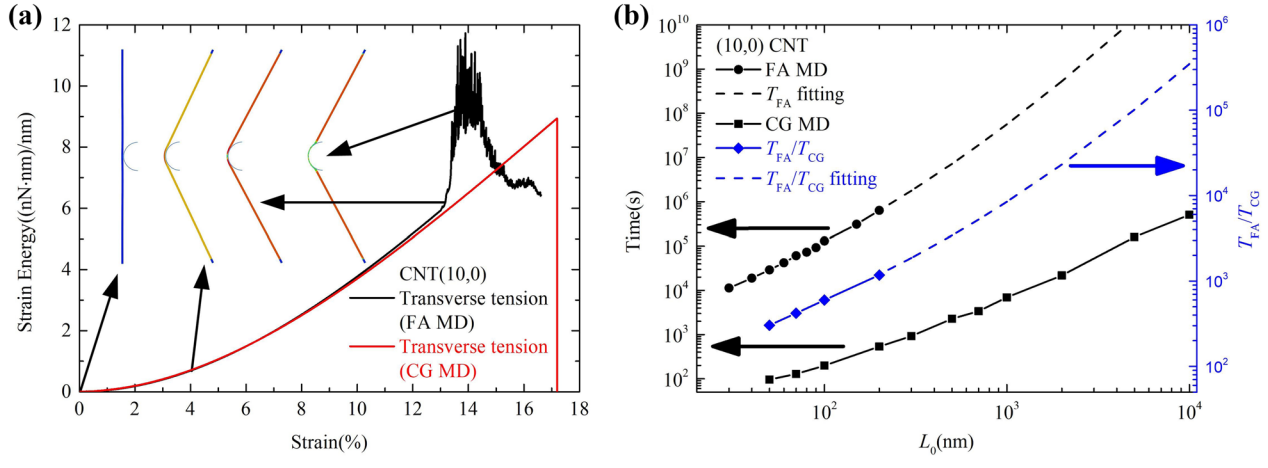

Figure 12 (**a**) Strain energy change of a (10,0) CNT under transverse tension, (**b**) The change of the computational cost of (10,0) CNT with different CNT length L_0 using FA MD and CG MD simulations [61]

Table 1 Multiscale theories and key mechanisms of CNT materials mentioned in this paper [43, 61, 73, 86, 94–96]

CNT materials	Multiscale theories	Key mechanisms
Bundles	Atom/continuum model	Structural instability
	Weibull distribution	Non-uniform strains
	CG MD	Chirality dependent
Networks	Monte Carlo	Crosslink density
	Graph theory	Connectivity problem
Films	CG molecular statics	Mean free path
Fibers	Multi-scale damage model	Strength loss

modulus, normal stiffness and Poisson's ratio, all within the transverse plane of a CNT bundle, using a model in which each tube is treated as a rigid continuum tube with perfectly circular cross-section and the intertube van der Waals interaction is modeled by the LJ potential. Liu et al. [94] presented a hybrid atom/continuum model to study the bulk elastic properties of SWNT bundles, and reported that CNT bundles may exhibit a transition in which the cross-sections of tubes turn from perfectly circular to hexagonal, depending upon the tube diameter and externally applied pressure, and this structural instability leads to an abrupt change in the bulk elastic properties of CNT bundles (Table 1).

Recently, centimeters-long CNT bundles with tensile strength over 80 GPa have been fabricated by Bai et al. [8, 95]. Using a synchronous tightening and relaxing (STR) strategy, the non-uniform initial strains of CNTs in the CNT bundle were released (Table 1). However, the failure mechanisms and the influence of CNT chirality were still unclear based on the experimental observations. Shortly afterwards, the above nonlinear CG potentials were used to simulate the mechanical behaviors

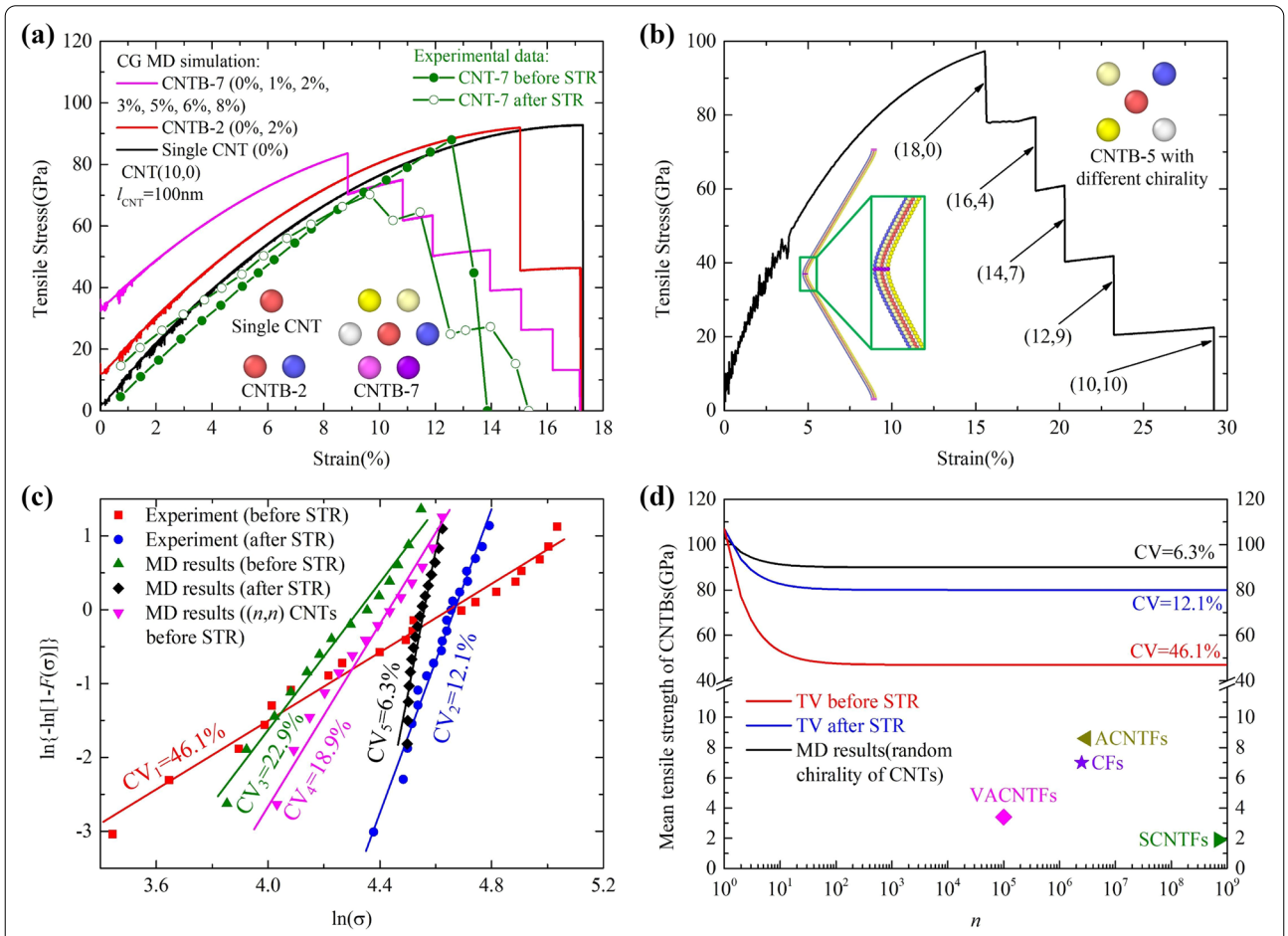

Figure 13 (**a**) The stress-strain curves of a single (10, 0) CNT, CNTB-2, CNTB-3 and CNTB-7 with different initial strains, (**b**) the stress-strain curves of the CNTB-5 (including (18,0), (16,4), (14,7), (12,9) and (10,10)), (**c**) the CV values of CNT bundles before and after the STR treatment and CG MD results, (**d**) the relationship between the mean tensile strength of CNTBs and their component number before and after STR treatment and CG MD results [8, 61]

of those ultralong CNT bundles [61]. Considering the non-uniform stresses of CNTs, the multi-stage stress-strain features of CNT bundles in the experiments were reproduced in CG MD simulations (Figure 13(a)). On the other hand, the ultimate strain of a CNT is determined by the CNT chirality from previous analytical results. Therefore, the influence of chirality was further studied. The multi-stage stress-strain features have also occurred even if there is no initial strain on every CNT of the CNT bundles (including (18,0), (16,4), (14,7), (12,9) and (10,10) CNTs) (Figure 13(b)). Based on the Weibull distribution, the strength distribution of individual CNTs in CNT bundles can be described by a coefficient of variation (CV, also called the coefficient of dispersion), which is the ratio of the standard deviation to the mean value of single CNT strength. A large CV value implies a highly dispersive distribution of the CNT strength. The CV values of CNT bundles from experiments and CG MD simulations are shown in Figure 13(c). Although the CV value of single CNTs decreases after the STR treatment, the strength distribution for individual CNTs of the CNT bundles with random chirality becomes narrowest. Figure 13(d) shows the experimentally measured and theoretically calculated tensile strength of CNT bundles before and after STR treatment. Statistic symbols at the bottom are the reported values for ACNTFs, CFs (carbon fibers), vertically aligned CNT arrays (VCNTFs) and spinning from CNT solutions (SCNTFs). In particular, the tensile strength of CNT bundles with random chiral CNTs using CG MD simulations is also shown Figure 13(d).

It is evident that with increasing n (the number of single CNTs in the CNT bundles), the mean tensile strength of the CNT bundles quasiexponentially decreases. The decrease rate of the strength decays with the increase in n, and finally, the mean tensile strength of the bundles reaches a constant value for n larger than a certain number. It is confirmed that the STR treatment can indeed improve the tensile strength as well as the breaking strain and toughness of CNT bundles. For as-synthesized CNT bundles without any treatment, when n is large enough, the mean tensile strength of the CNT bundles can be as low as about 47 GPa. In contrast, the mean tensile strength of CNT bundles with large n is as high as 80 GPa after the STR treatment. In particular, the mean tensile strength of CNT bundles (including random chiral CNTs) with large n can be up to 90 GPa.

Owing to the reinforcement of intertube connection by the crosslinks, CNT networks with different crosslink densities exhibit numerous outstanding yet quite divergent mechanical properties, such as stiffness and softness, brittleness and ductility, and elasticity and plasticity. Although the crosslinks play a key role in the load transfer of CNT networks, understanding of the crosslink determined mechanical properties is still mainly phenomenological and lacks a unified physical explanation. Using the coarse-grained molecular dynamics simulations, Ji et al. [96] reported that the load transfer in CNT networks is determined by the crosslink density via three critical thresholds, namely, percolation, connection, and saturation, which divide the transfer into four different modes. Reminiscent of the connectivity problem in the graph theory, an individual path for the successive load transfer through the network is formed at the first threshold, then all CNTs are connected by crosslinks at the second one, and finally, the connections are gradually converted into tetrahedrons toward rigidized connectivity until the third saturation threshold. This study systematically establishes the relationship among crosslink-density dependent structural characteristics, load-transfer ways, and mechanical behaviors of CNT networks, which should provide insight into modulating the mechanical properties of fibrous materials through the design of microstructures.

5 Conclusions

In this paper, a thorough literature review of multiscale analyses for CNT network materials is presented, with a focus on the microstructural characteristics and load transfer mechanisms. Because of the microstructural complexity and hierarchy, multiscale analyses were conducted to reveal the load transfer mechanisms and establish the structure-property relationships in CNT networks. Based on the molecular mechanics models, the tensile behaviors of a single CNT are correlated with tube chirality and stress localization. CNTs preferably form locally closely-packed bundles and exhibit a certain stacking order due to the inter-tube vdW interactions. Due to the finite length of CNTs, the tensile strength of a bundle can be determined by the shear stresses between CNTs, the degree of alignment and the number of CNTs in the CNT bundle. To reduce the computational cost, a mesoscale model was developed to study the nonlinear mechanical behaviors of CNT networks. By extracting a few key parameters that capture the microstructures of CNT networks and relating them to the fabrication process, multiple methods (including introducing the covalent crosslinks between CNTs, releasing the non-uniform initial strains and increasing the alignment degree of CNTs) are proposed to improve the mechanical properties of CNT network materials.

Although CNT networks have shown superior mechanical and conductive properties than traditional materials, the extraordinary properties of individual CNTs have not yet been fully transferred in network materials from nano-scale to macro-scale. Understanding the fundamentals of the

processing–structure–property relationship of CNT network materials is a prerequisite for their optimizations. As presented in this review, the basics of the dependence of mechanical properties on network structures have been widely investigated. However, the load-transfer mechanisms in multi-scale levels are discussed separately, which are coupled in practice. For example, tuning the interfacial interaction between individual CNTs or CNT bundles by creating crosslinks between surface functional groups inevitably reduces the mechanical resistance of the CNTs or bundles. These facts could be discussed by generalizing the theory presented in this work. The understanding of the linkage between processing and structures is another challenge. Some prominent obstacles, such as synthesis, purification, large-scale production, and assembly into devices, severely hamper further development in this field and need much more dedicated efforts in the future.

Acknowledgements
Not applicable.

Author Contributions
JH put forward the framework and content of the paper; JC wrote the manuscript; YL assisted in data collection. CH and AP assisted in modifying the structure and content of this paper. All authors read and approved the final manuscript.

Authors' Information
Jiachao Ji, born in 1993, is currently a PhD candidate at *Jiangsu Key Laboratory of Advanced Food Manufacturing Equipment and Technology, Jiangnan University, China*. He received his bachelor's degree from *Changzhou University, China*, in 2016. His research interests include nanomechanics and advanced materials.
Yulin Jin, born in 1997, is currently a graduate student at *Jiangnan University, China*. He received his bachelor's degree from *Northwest Agriculture & Forestry University, China*, in 2020.
Anping Hua, born in 1996, is currently a PhD candidate at *Jiangsu Key Laboratory of Advanced Food Manufacturing Equipment and Technology, Jiangnan University, China*.
Chunhua Zhu, born in 1993, is currently a PhD candidate at *Jiangsu Key Laboratory of Advanced Food Manufacturing Equipment and Technology, Jiangnan University, China*. He received his bachelor's degree from *Jiangnan University, China*, in 2016. His research interests include nanomechanics and advanced materials.
Junhua Zhao, born in 1979, is currently a professor and a PhD candidate supervisor at *Jiangsu Key Laboratory of Advanced Food Manufacturing Equipment and Technology, Jiangnan University, China*. His main research interests include fracture mechanics, nanomechanics, 3D-printing technology and advanced materials.

Funding
Supported by National Natural Science Foundation of China (Grant Nos. 11972171, 11572140), Sixth Phase of Jiangsu Province "333 High Level Talent Training Project" Second Level Talents, 111 Project (Grant No. B18027), Natural Science Foundation of Jiangsu Province (Grant No. BK20180031), Research Project of State Key Laboratory of Mechanical System and Vibration (Grant No. MSV201909), Fundamental Research Funds for the Central Universities (Grant No. JUSRP22002), Postgraduate Research & Practice Innovation Program of Jiangsu Province (Grant No. KYCX19_1861).

Competing Interests
The authors declare no competing financial interests.

Author Details
[1]Jiangsu Key Laboratory of Advanced Food Manufacturing Equipment and Technology, Jiangnan University, Wuxi 214122, China. [2]Institute of Mechanics and Advanced Materials, School of Mechanical Engineering, Jiangnan University, Wuxi 214122, China.

Received: 27 February 2022 Revised: 11 August 2022 Accepted: 7 December 2022
Published online: 05 January 2023

References

[1] X F Zhang, Q W Li, T G Holesinger, et al. Ultrastrong, stiff, and lightweight carbon-nanotube fibers. *Advanced Materials*, 2007, 19(23): 4198.
[2] S Iijima. Helical microtubules of graphitic carbon. *Nature*, 1991, 354(6348): 56-58.
[3] B I Yakobson, C J Brabec, J Bernholc. Nanomechanics of carbon tubes: Instabilities beyond linear response. *Physical Review Letters*, 1996, 76(14): 2511-2514.
[4] L P Yu, X H Zhou, L Lu, et al. MXene/carbon nanotube hybrids: synthesis, structures, properties, and applications. *Chemsuschem*, 2021, 14(23): 5079-5111.
[5] R S Ruoff, D Qian, W K Liu. Mechanical properties of carbon nanotubes: theoretical predictions and experimental measurements. *Comptes Rendus Physique*, 2003, 4(9): 993-1008.
[6] B Vigolo, A Penicaud, C Coulon, et al. Macroscopic fibers and ribbons of oriented carbon nanotubes. *Science*, 2000, 290(5495): 1331-1334.
[7] A B Dalton, S Collins, E Munoz, et al. Super-tough carbon-nanotube fibres - These extraordinary composite fibres can be woven into electronic textiles. *Nature*, 2003, 423(6941): 703-703.
[8] Y X Bai, R F Zhang, X Ye, et al. Carbon nanotube bundles with tensile strength over 80 GPa. *Nature Nanotechnology*, 2018, 13(7): 589.
[9] J T Di, X H Zhang, Z Z Yong, et al. Carbon-nanotube fibers for wearable devices and smart textiles. *Advanced Materials*, 2016, 28(47): 10529-10538.
[10] X H Zhang, W B Lu, G H Zhou, et al. Understanding the mechanical and conductive properties of carbon nanotube fibers for smart electronics. *Advanced Materials*, 2020, 32(5): 1902028.
[11] L J Hall, V R Coluci, D S Galvao, et al. Sign change of Poisson's ratio for carbon nanotube sheets. *Science*, 2008, 320(5875): 504-507.
[12] Y Chen, L Zhang, H Zhan, et al. New processing method to fabricate high-performance carbon-nanotube/polyvinyl alcohol composite films. *Carbon*, 2016, 110: 490-496.
[13] X C Gui, J Q Wei, K L Wang, et al. Carbon nanotube sponges. *Advanced Materials*, 2010, 22(5): 617.
[14] W Q Zhao, H Zhang, J Liu, et al. Controlled air-etching synthesis of porous-carbon nanotube aerogels with ultrafast charging at 1000 A g(-1). *Small*, 2018, 14(40): 1802394.
[15] X Q Yang, J N Zhao, K J Wu, et al. Making a strong adhesion between polyetherketoneketone and carbon nanotube fiber through an electro strategy. *Composites Science and Technology*, 2019, 177: 81-87.
[16] Y H Song, J T Di, C Zhang, et al. Millisecond tension-annealing for enhancing carbon nanotube fibers. *Nanoscale*, 2019, 11(29): 13909-13916.
[17] Y X Gao, H W Chen, J Ge, et al. Direct intertube cross-linking of carbon nanotubes at room temperature. *Nano Letters*, 2016, 16(10): 6541-6547.
[18] O K Park, H Choi, H Jeong, et al. High-modulus and strength carbon nanotube fibers using molecular cross-linking. *Carbon*, 2017, 118: 413-421.
[19] R J Mora, J J Vilatela, A H Windle. Properties of composites of carbon nanotube fibres. *Composites Science and Technology*, 2009, 69(10): 1558-1563.
[20] R D Downes, A Hao, J G Park, et al. Geometrically constrained self-assembly and crystal packing of flattened and aligned carbon nanotubes. *Carbon*, 2015, 93: 953-966.
[21] Z P Huang, J W Wu, Z F Ren, et al. Growth of highly oriented carbon nanotubes by plasma-enhanced hot filament chemical vapor deposition. *Applied Physics Letters*, 1998, 73(26): 3845-3847.
[22] Z F Ren, Z P Huang, J W Xu, et al. Synthesis of large arrays of well-aligned carbon nanotubes on glass. *Science*, 1998, 282(5391): 1105-1107.
[23] Y L Li, I A Kinloch, A H Windle. Direct spinning of carbon nanotube fibers from chemical vapor deposition synthesis. *Science*, 2004, 304(5668): 276-278.

[24] M Zhang, K R Atkinson, R H Baughman. Multifunctional carbon nanotube yarns by downsizing an ancient technology. *Science*, 2004, 306(5700): 1358-1361.

[25] J Hone, M C Llaguno, N M Nemes, et al. Electrical and thermal transport properties of magnetically aligned single walt carbon nanotube films. *Applied Physics Letters*, 2000, 77(5): 666-668.

[26] X Q Chen, T Saito, H Yamada, et al. Aligning single-wall carbon nanotubes with an alternating-current electric field. *Applied Physics Letters*, 2001, 78(23): 3714-3716.

[27] K Koziol, J Vilatela, A Moisala, et al. High-performance carbon nanotube fiber. *Science*, 2007, 318(5858): 1892-1895.

[28] Q F Cheng, J W Bao, J Park, et al. High mechanical performance composite conductor: multi-walled carbon nanotube sheet/bismaleimide nanocomposites. *Advanced Functional Materials*, 2009, 19(20): 3219-3225.

[29] M Menon, A N Andriotis, D Srivastava, et al. Carbon nanotube "T junctions": Formation pathways and conductivity. *Physical Review Letters*, 2003, 91: 145501.

[30] A Kis, G Csanyi, J P Salvetat, et al. Reinforcement of single-walled carbon nanotube bundles by intertube bridging. *Nature Materials*, 2004, 3(3): 153-157.

[31] M Barrejon, R Rauti, L Ballerini, et al. Chemically cross-linked carbon nanotube films engineered to control neuronal signaling. *Acs Nano*, 2019, 13(8): 8879-8889.

[32] T Filleter, H D Espinosa. Multi-scale mechanical improvement produced in carbon nanotube fibers by irradiation cross-linking. Carbon, 2013, 56(1): 11.

[33] E R Meshot, D W Zwissler, N Bui, et al. Quantifying the hierarchical order in self-aligned carbon nanotubes from atomic to micrometer scale. *Acs Nano*, 2017, 11(6): 5405-5416.

[34] Q Li, J S Wang, Y L Kang, et al. Multi-scale study of the strength and toughness of carbon nanotube fiber materials. *Materials Science and Engineering A*, 2012, 549: 118-122.

[35] S M Cooper, H F Chuang, M Cinke, et al. Gas permeability of a buckypaper membrane. *Nano Letters*, 2003, 3(2): 189-192.

[36] Q Li, Y L Kang, W Qiu, et al. Deformation mechanisms of carbon nanotube fibres under tensile loading by in situ Raman spectroscopy analysis. *Nanotechnology*, 2011, 22: 225704.

[37] W L Deng, W Qiu, Q Li, et al. Multi-scale experiments and interfacial mechanical modeling of carbon nanotube fiber. *Experimental Mechanics*, 2014, 54(1): 3-10.

[38] C Jolowsky, R Sweat, J G Park, et al. Microstructure evolution and self-assembling of CNT networks during mechanical stretching and mechanical properties of highly aligned CNT composites. *Composites Science and Technology*, 2018, 166: 125-130.

[39] R Downes, S K Wang, D Haldane, et al. Strain-induced alignment mechanisms of carbon nanotube networks. *Advanced Engineering Materials*, 2015, 17(3): 349-358.

[40] Y N Zhang, L X Zheng, G Z Sun, et al. Failure mechanisms of carbon nanotube fibers under different strain rates. *Carbon*, 2012, 50(8): 2887-2893.

[41] G Z Sun, L X Zheng, J Y Zhou, et al. Load-transfer efficiency and mechanical reliability of carbon nanotube fibers under low strain rates. *International Journal of Plasticity*, 2013, 40: 56-64.

[42] G Z Sun, J H L Pang, J Y Zhou, et al. A modified Weibull model for tensile strength distribution of carbon nanotube fibers with strain rate and size effects. *Applied Physics Letters*, 2012, 101: 131905.

[43] E L Gao, W B Lu, Z P Xu. Strength loss of carbon nanotube fibers explained in a three-level hierarchical model. *Carbon*, 2018, 138: 134-142.

[44] M M J Treacy, T W Ebbesen, J M Gibson. Exceptionally high Young's modulus observed for individual carbon nanotubes. *Nature*, 1996, 381(6584): 678-680.

[45] M F Yu, O Lourie, M J Dyer, et al. Strength and breaking mechanism of multiwalled carbon nanotubes under tensile load. *Science*, 2000, 287(5453): 637-640.

[46] C Q Ru. Effective bending stiffness of carbon nanotubes. *Physical Review B*, 2000, 62(15): 9973-9976.

[47] C Q Ru. Effect of van der Waals forces on axial buckling of a double-walled carbon nanotube. *Journal of Applied Physics*, 2000, 87(10): 7227-7231.

[48] J Z Liu, Q S Zheng, Q Jiang. Effect of a rippling mode on resonances of carbon nanotubes. *Physical Review Letters*, 2001, 86(21): 4843-4846.

[49] L F Wang, Q S Zheng, Q Jiang. Size dependence of the thin-shell model for carbon nanotubes. *Physical Review Letters*, 2005, 95: 105501.

[50] C Y Li, T W Chou. A structural mechanics approach for the analysis of carbon nanotubes. *International Journal of Solids and Structures*, 2003, 40(10): 2487-2499.

[51] C Y Li, T W Chou. Elastic properties of single-walled carbon nanotubes in transverse directions. *Physical Review B*, 2004, 69: 073401.

[52] N A Kasti. Zigzag carbon nanotubes - Molecular/structural mechanics and the finite element method. *International Journal of Solids and Structures*, 2007, 44(21): 6914-6929.

[53] G M Odegard, T S Gates, L M Nicholson, et al. Equivalent-continuum modeling of nano-structured materials. *Composites Science and Technology*, 2002, 62(14): 1869-1880.

[54] T C Chang, H J Gao. Size-dependent elastic properties of a single-walled carbon nanotube via a molecular mechanics model. *Journal of the Mechanics and Physics of Solids*, 2003, 51(6): 1059-1074.

[55] T C Chang, G Q Li, X M Guo. Elastic axial buckling of carbon nanotubes via a molecular mechanics model. *Carbon*, 2005, 43(2): 287-294.

[56] J Y Geng, T C Chang. Nonlinear stick-spiral model for predicting mechanical behavior of single-walled carbon nanotubes. *Physical Review B*, 2006, 74: 245428.

[57] J H Zhao, L F Wang, J W Jiang, et al. A comparative study of two molecular mechanics models based on harmonic potentials. *Journal of Applied Physics*, 2013, 113: 063509.

[58] J H Zhao, W L Guo, T Rabczuk. An analytical molecular mechanics model for the elastic properties of crystalline polyethylene. *Journal of Applied Physics*, 2012, 112: 033516.

[59] A Favata, A Micheletti, P Podio-Guidugli, et al. Geometry and self-stress of single-wall carbon nanotubes and graphene via a discrete model based on a 2nd-generation REBO potential. *Journal of Elasticity*, 2016, 125(1): 1-37.

[60] D W Brenner, O A Shenderova, J A Harrison, et al. A second-generation reactive empirical bond order (REBO) potential energy expression for hydrocarbons. *Journal of Physics-Condensed Matter*, 2002, 14(4): 783-802.

[61] J C Ji, J H Zhao, W L Guo. Novel nonlinear coarse-grained potentials of carbon nanotubes. *Journal of the Mechanics and Physics of Solids*, 2019, 128: 79-104.

[62] D Q Ding, Y Zhao, S H Dong, et al. The vibration of a linear carbon chain in carbon nanotubes. *Materials*, 2017, 10(5): 478.

[63] R M Liu, J H Zhao, L F Wang. Flexural wave propagation in mass chain-filled carbon nanotubes. *Materials*, 2019, 12(18): 2986.

[64] C H Zhu, Y F Chen, R M Liu, et al. Buckling behaviors of single-walled carbon nanotubes inserted with a linear carbon-atom chain. *Nanotechnology*, 2018, 29: 335704.

[65] L Y Jiang, Y Huang, H Jiang, et al. A cohesive law for carbon nanotube/polymer interfaces based on the van der Waals force. *Journal of the Mechanics and Physics of Solids*, 2006, 54(11): 2436-2452.

[66] W B Lu, J Wu, J Song, et al. A cohesive law for interfaces between multi-wall carbon nanotubes and polymers due to the van der Waals interactions. *Computer Methods in Applied Mechanics and Engineering*, 2008, 197(41-42): 3261-3267.

[67] C Y Wang, Y Y Zhang, C M Wang, et al. Buckling of carbon nanotubes: A literature survey. *Journal of Nanoscience and Nanotechnology*, 2007, 7(12): 4221-4247.

[68] J H Zhao, J W Jiang, Y Jia, et al. A theoretical analysis of cohesive energy between carbon nanotubes, graphene and substrates. *Carbon*, 2013, 57: 108-119.

[69] J H Zhao, Y Jia, N Wei, et al. Binding energy and mechanical stability of two parallel and crossing carbon nanotubes. *Proceedings of the Royal Society A-Mathematical Physical and Engineering Sciences*, 2015, 471: 2180.

[70] Y F Chen, D Q Ding, C H Zhu, et al. Size- and edge-effect cohesive energy and shear strength between graphene, carbon nanotubes and nanofibers: Continuum modeling and molecular dynamics simulations. *Composite Structures*, 2019, 208: 150-167.

[71] J S Soares, A P M Barboza, P T Araujo, et al. Modulating the electronic properties along carbon nanotubes via tube-substrate interaction. *Nano Letters*, 2010, 10(12): 5043-5048.

[72] J H Zhao, L X Lu, T Rabczuk. Binding energy and mechanical stability of single- and multi-walled carbon nanotube serpentines. *Journal of Chemical Physics*, 2014, 140: 204704.
[73] C X Li, Y L Liu, Q S Zheng. Interfacial shear strengths between carbon nanotubes. *Nanotechnology*, 2010, 21: 115704.
[74] D Q Ding, Z Y Yang, S H Dong, et al. Thermo-mechanical vibration of a single-layer graphene sheet and a single-walled carbon nanotube on a substrate. *Journal of Applied Physics*, 2017, 121: 094304.
[75] Y Li, Y Xiong, Z K Zhou, et al. The peeling behavior of nanowires and carbon nanotubes from a substrate using continuum modeling. *Journal of Applied Physics*, 2017, 121: 054303.
[76] S H Dong, C H Zhu, Y F Chen, et al. Buckling behaviors of metal nanowires encapsulating carbon nanotubes by considering surface/interface effects from a refined beam model. *Carbon*, 2019, 141: 348-362.
[77] L V Zhigilei, C Wei, D Srivastava. Mesoscopic model for dynamic simulations of carbon nanotubes. *Physical Review B*, 2005, 71: 165417.
[78] M J Buehler. Mesoscale modeling of mechanics of carbon nanotubes: Self-assembly, self-folding, and fracture. *Journal of Materials Research*, 2006, 21(11): 2855-2869.
[79] S W Cranford, M J Buehler. In silico assembly and nanomechanical characterization of carbon nanotube buckypaper. *Nanotechnology*, 2010, 21: 265706.
[80] J H Zhao, J W Jiang, L F Wang, et al. Coarse-grained potentials of single-walled carbon nanotubes. *Journal of the Mechanics and Physics of Solids*, 2014, 71: 197-218.
[81] J H Zhao, P S Yu, S H Dong. The influence of crosslink density on the failure behavior in amorphous polymers by molecular dynamics simulations. *Materials*, 2016, 9(4): 234.
[82] B Xie, Y L Liu, Y T Ding, et al. Mechanics of carbon nanotube networks: microstructural evolution and optimal design. *Soft Matter*, 2011, 7(21): 10039-10047.
[83] C Wang, B Xie, Y L Liu, et al. Mechanotunable microstructures of carbon nanotube networks. *Acs Macro Letters*, 2012, 1(10): 1176-1179.
[84] C Wang, L F Wang, Z P Xu. Enhanced mechanical properties of carbon nanotube networks by mobile and discrete binders. *Carbon*, 2013, 64: 237-244.
[85] C Wang, E L Gao, L F Wang, et al. Mechanics of network materials with responsive crosslinks. *Comptes Rendus Mecanique*, 2014, 342(5): 264-272.
[86] T Yang, C Wang, Z B Wu. Crosslink-tuned large-deformation behavior and fracture mode in buckypapers. *Carbon*, 2020, 159: 412-421.
[87] A Banna, K W Kayang, A N Volkov. Effects of the nanotube length and network morphology on the deformation mechanisms and mechanical properties of cross-linked carbon nanotube films. *Journal of Applied Physics*, 2021, 129: 105101.
[88] A N Volkov, A Banna. Mesoscopic computational model of covalent cross-links and mechanisms of load transfer in cross-linked carbon nanotube films with continuous networks of bundles. *Computational Materials Science*, 2020, 176: 109410.
[89] Y L Chen, F Pan, Z Y Guo, et al. Stiffness threshold of randomly distributed carbon nanotube networks. *Journal of the Mechanics and Physics of Solids*, 2015, 84: 395-423.
[90] F Pan, Y L Chen, Q H Qin. Stiffness thresholds of buckypapers under arbitrary loads. *Mechanics of Materials*, 2016, 96: 151-168.
[91] L H Jin, A Chortos, F F Lian, et al. Microstructural origin of resistance-strain hysteresis in carbon nanotube thin film conductors. *Proceedings of the National Academy of Sciences of the United States of America*, 2018, 115(9): 1986-1991.
[92] J P Salvetat, G Briggs, J M Bonard et al. Elastic and shear moduli of single-walled carbon nanotube ropes. *Physical Review Letters*, 1999, 82(5): 944-947.
[93] E Saether, S Frankland, R B Pipes. Transverse mechanical properties of single-walled carbon nanotube crystals. Part I: determination of elastic moduli. *Composites Science and Technology*, 2003, 63(11): 1543–1550.
[94] J Z Liu, Q S Zheng, Q Zhang. Mechanical properties of single-walled carbon nanotube bundles as bulk materials. *Journal of the Mechanics and Physics of Solids*, 2005, 53(1): 123-142.
[95] Y X Bai, H J Yue, J Wang, et al. Super-durable ultralong carbon nanotubes. *Science*, 2020, 369(6507): 1104.
[96] J C Ji, J J Wang, C H Zhu, et al. Revealing density thresholds of carbon nanotube cross-links for load transfer: a graph theory strategy. *ACS Nano*, 2022, 16(4): 6929-6936.